Short communication

The role of temperature on the corrosion and passivation of type 310S stainless steel in eutectic (Li + K) carbonate melt

S. Frangini [a,*], S. Loreti [b]

[a] ENEA C.R.E. Casaccia, IDROCOMB, Via Anguillarese 301, 00060 Rome, Italy
[b] ENEA C.R. Frascati, FIS-LAS, Via Enrico Fermi 45, 00044 Frascati, Rome, Italy

Abstract

The corrosion behavior of type 310S stainless steel was studied in the eutectic Li + K carbonate as a function of temperature by several electrochemical methods. Within the range 600–675 °C the steel passivated spontaneously at OCP condition after a few hours of immersion. Active-passive transition was observed in the polarization curves below 600 °C and above 675 °C indicating a failure to reach a stable passive condition even at prolonged exposure times. Impedance analysis indicates that passivity does not lead to the formation of an impervious barrier layer as denoted by the presence of diffusional components at low frequencies indicating oxide growth. Corrosion rates exhibited a minimum at 675 °C at both OCP and at cathode polarization conditions. A mechanism to explain the active–passive transition has been proposed based on the phase transition from $LiFe_5O_8$ to $LiFeO_2$.
© 2006 Elsevier B.V. All rights reserved.

Keywords: 310S stainless steel; Li + K carbonate; Passivation; Impedance spectra; Anodic polarization

1. Introduction

Austenitic 316L and 310S stainless steels are the most commonly used materials for the construction of bipolar plate components in the molten carbonate fuel cell (MCFC) technology because of good compromise between corrosion resistance and oxide scale resistivity at 650 °C under standard operating conditions. In detail, type 310S steel exhibits a much slower oxide growth rate, although 316L steel is sometimes preferred as its oxide scale has a higher electrical conductivity [1]. The corrosion resistance of these steels basically relies on the rapid formation of a protective passive oxide scale that is able to suppress the outward diffusion of base-metal cations (mainly, iron) into the molten electrolyte. After long test periods, the two-layered structure of the passive scale consists of an external $LiFeO_2$ layer and an inner Cr-rich oxide layer. The passivity of stainless steels depends on the stability of this inner layer [1,2]. In the case of the high-Cr type 310S steel (ca. 25 wt.%), the Cr-rich oxide layer is composed mainly of a compact, thin and corrosion resistant layer of $LiCrO_2$ which strongly hinders the iron diffusion, thus limiting the growth of the external $LiFeO_2$ layer. Conversely, the 316L steel forms higher inner conductive spinel layer mainly consisting of $LiFe_5O_8$ and $FeCrO_4$ phases. The spinel layer is less effective in retarding the outer iron diffusion, thus leading to a faster growth of the external $LiFeO_2$ layer and to an overall higher thickness of the scale [1,3].

Since MCFC stack operations result in large temperature variations (580–700 °C) along the surface of bipolar plates it would be important to evaluate the steel corrosion as a function of temperature, although this aspect has been scarcely investigated in literature. For instance, the authors of Refs. [2,4] report that the corrosion of 316L steel becomes highly sensitive on the reaction conditions in the eutectic Li + Na carbonate melt during cell start-up. At temperatures as low as 600 °C this steel seems to become highly susceptible to corrosion damage with a pitting-like attack in high CO_2 gases. Obviously, the possibility of a localized corrosion is a real concern for the use of the 316L steel in alternative alkali carbonate compositions based on the Li + Na electrolyte.

As part of a work aimed to analyze the corrosion behavior of 316L and 310S steels in Li + K and Li + Na carbonates, we will present some results on the stability of the passive scale forming on the 310S stainless steel surface in Li + K melt in the temperature range 580–700 °C. This study has been mainly conducted by electrochemical methods with emphasis to the measurements of

* Corresponding author. Tel.: +39 06 30483138; fax: +39 06 30483327.
 E-mail address: frangini@casaccia.enea.it (S. Frangini).

open circuit potential, anodic polarization curves and impedance spectra.

2. Experimental

Working electrodes for the electrochemical measurements were machined from a 1-mm thick sheet of commercial type 310S austenitic stainless steel. The electrodes were shaped to 10 mm × 10 mm squares. The surface of the samples was mechanically polished with water-cooled SiC paper up to 600 grit with the residues removed by a short ultrasound treatment in high-purity water. The electrode holder was made by spot welding the sample back face to a gold lead wire, which was inserted in a thin alumina tube. The back face was then sealed with alumina cement. A gold foil (10 mm × 10 mm) was used as counter-electrode, whereas a gold wire dipped in the eutectic $(0.62Li + 0.38K)_2CO_3$ mixture under CO_2–O_2 gas (0.667–0.333 atm) and contained in a alumina tube served as oxygen reference electrode. The liquid contact with the working electrode compartment was assured by a small pinhole in the reference tube.

The apparatus for electrochemical experiments consisted in an alumina pot-cell as described elsewhere [5]. The electrolyte used for this work consisted in a solution of Li_2CO_3 and K_2CO_3 salts mixed at the eutectic composition (62 mol% Li_2CO_3 and 38 mol% K_2CO_3). Fifty grams of salt were used to ensure that the electrodes were totally immersed in the electrolyte during experiments. All gas mixtures were at a total pressure of 1 atm. The total gas flowrate was set a $100\,cm^3\,min^{-1}$ by an Aalborg thermal mass flowmeter.

The electrochemical measurements were made by using computer-controlling equipments consisting of a potentiostat/galvanostat (EG&G 173) and a lock-in amplifier (EG&G 5301). Polarization scans were carried out at a rate of $1\,mV\,s^{-1}$. EIS measurements were carried out at OCP conditions with the fast Fourier transform (FFT) technique instead of the more time-consuming single-sine technique.

After the corrosion tests analysis of the corrosion products was conducted by XRD on selected electrodes.

3. Results and discussion

3.1. Open circuit potential (OCP) measurements

The OCP variation of type 310S stainless steel at various temperatures of relevance to MCFC was followed as a function of immersion time until a steady state condition is established (Fig. 1). It is known that such kinds of measurements can provide useful information on the formation of stable passive scale taking into account that metallic corrosion in molten salts can be usually described as the sum of two basic processes, namely anodic metal oxidation (eventually leading to passivation) and oxide scale dissolution.

Thus, from Fig. 1 we can observe that OCP reaches a stable condition with increasing anodic values at increased temperature in the range 575–675 °C, whereas at 695 °C the OCP falls in the cathodic direction at a value lower than that at 575 °C.
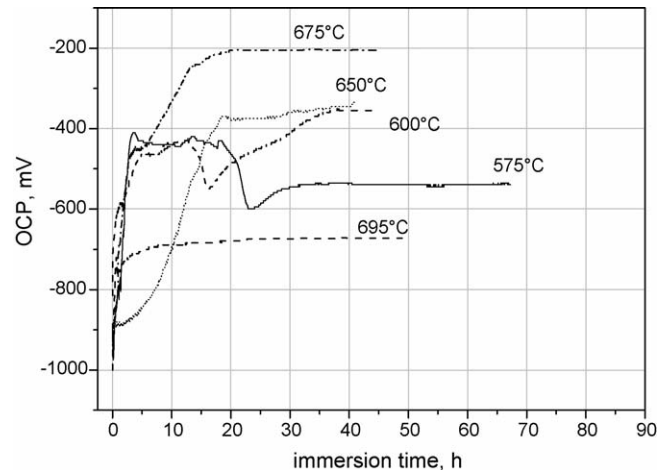

Fig. 1. OCP of type 310S stainless steel as a function of temperature in the Li + K carbonate under standard cathode gas.

These facts indicate a temperature raising from 575 to 675 °C favours the onset of passivity and a general corrosion resistance improvement. On the other hand, the OCP behavior at 695 °C is a clear indication of some dissolution of the oxide scale thus leading to a degradating protectiveness of the steel surface.

3.2. Polarization curves

The use of short-term polarization tests for life-time prediction is mainly based on the assumption that the same corrosion process should hold good over a long time span. This may be not true for alloys such as type 310S steel that rapidly develop increasing corrosion resistance over the time. Therefore, polarization curves were acquired at the end of OCP experiments when a stationary surface condition was clearly reached.

Polarization scans were observed to deeply alter the surface of the passive steel electrode in molten carbonates for currents exceeding several $mA\,cm^{-2}$ [6]. Care was therefore taken to acquire curves avoiding large cathodic overpotentials and ending anodic scans at 0 mV. However, for actively corroding electrodes such as the sample at 695 °C, surface perturbations induced by deep polarization were less evident.

Fig. 2 illustrates the potentiodynamic polarization response of type 310S at various temperatures. Active–passive transition was clearly observed at both 575 and 695 °C indicating that at these temperatures the steel was not able to reach a passive condition under OCP. Conversely, the polarization curves in the range 600–675 °C showed a fully passive behavior with similar passive current densities. The active–passive peak are observed at about −350 mV.

3.3. Potential decay measurements

The absence of passivity at 695 °C was also confirmed by potential decay measurements. On stable electrodes an anodic current of $10\,mA\,cm^{-2}$ was applied for 1 min to create strong melt acidity conditions, i.e. production of CO_2. Due to the slow recombination reaction ($CO_2 + O^{2-} = CO_3^{2-}$), this treatment
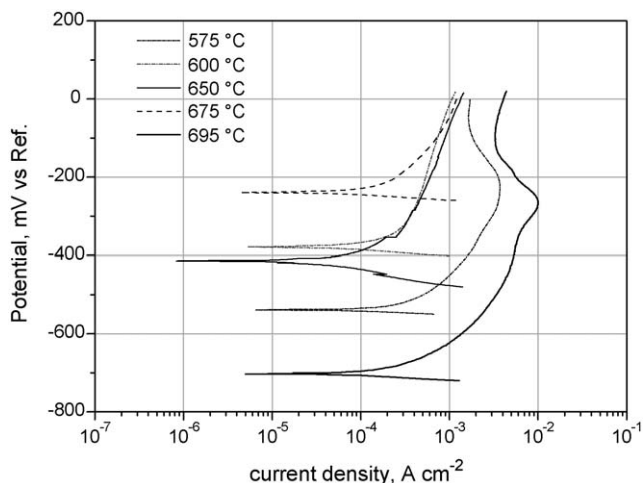
Fig. 2. Polarization curves of type 310S electrode at various temperatures in the Li + K carbonate under standard cathode gas. Scan rate: 1 mV s^{-1}.
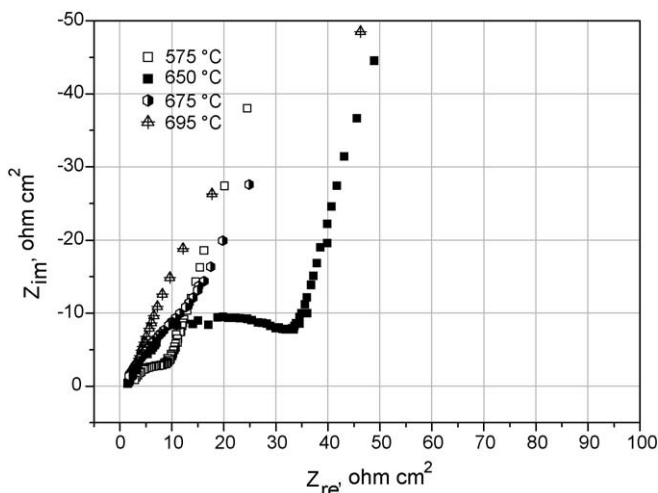

Fig. 4. Impedance spectra of type 310S stainless steel in the Li + K carbonate under standard cathode gas recorded at stable OCP conditions.
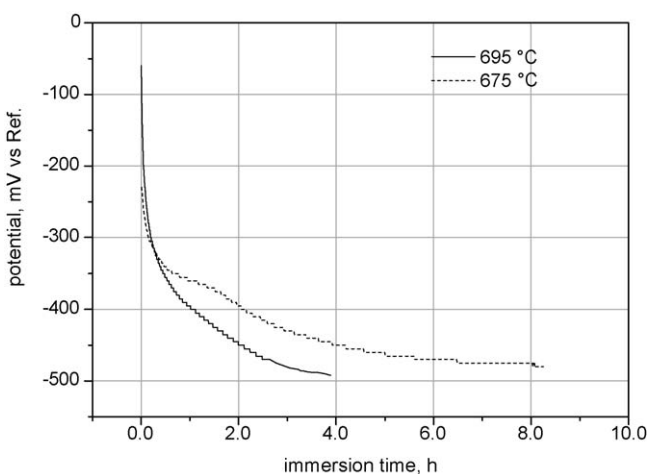

Fig. 3. OCP decay recorded at two different temperatures. The type 310S electrode was held at 10 mA cm^{-2} for 1 m in the Li + K carbonate under standard cathode gas.

of Li$^+$ ions in the nickel oxide structure [7], it seems reasonable to conclude that Ni^{2+} ion formation during depassivation should also correspond to a delithiation of the oxide scale. Conversely, as any reactivation process is hardly detectable at 695 °C this may only signify that a passive scale was not originally present on the electrode surface and that in general passivity breakdown should be somewhat related to a delithiation process of the oxide scale. Interestingly, from the polarization curves of Fig. 2 it is noted that the active–passive peak falls in the same potential region of the reactivation curve giving further support to this hypothesis.

3.4. Impedance spectra

As for polarization curves, impedance spectra were similarly recorded at the end of OCP experiments under stable potential conditions. They were measured at 575, 650, 675 and 695 °C as shown in Fig. 4. The partially resolved semicircle observable in the higher frequency region of the spectra at 575–675 °C may in general indicate presence of non-diffusional components (i.e. interfacial charge transfer, ion transport across the scale). Conversely, the linear impedance response at 695 °C indicates that corrosion is largely dominated by diffusional components. The spectra were best fitted with an equivalent circuit similar to that reported in [8] by using the Boukamp Equivalent Circuit Analysis software. The circuit is shown in Fig. 5. The results of the fit procedure are presented in Table 1. The constant phase element (CPE) represented by the pre-exponential factor Q and by the

was suitable to destabilize any passive film initially present on the surface. Thereafter, the potential decay was started to record. Fig. 3 reports an example of such measurements conducted at 675 and 695 °C. In the plot a well-defined potential arrest at -350 mV is visible only for the electrode heated at 675 °C, thus confirming that an initial passive film was actually present on the electrode surface. This potential arrest must be indicative of some electro-reduction process taking place during depassivation that could be ascribed to reduction of Ni^{3+} to Ni^{2+} ions. In fact, as the inverse process is known to favour the accomodation

Table 1
Fitting parameters obtained with the equivalent circuit of Fig. 5

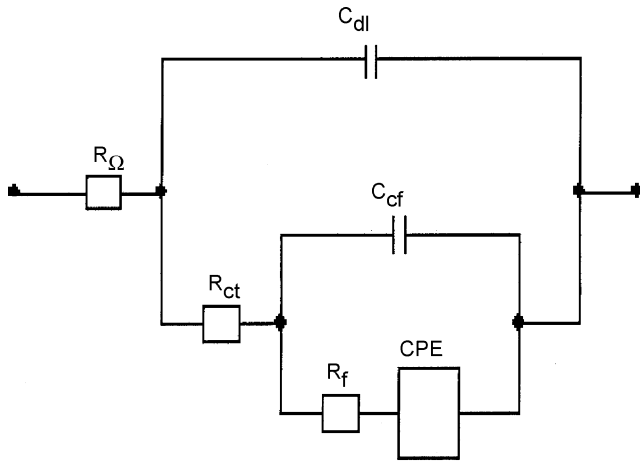| T (°C)	R_Ω ($\Omega\,cm^2$)	C_{dl} (F cm^{-2})	R_{ct} ($\Omega\,cm^2$)	C_f (F cm^{-2})	R_f ($\Omega\,cm^2$)	Q (s$^n\,\Omega^{-1}$)	n	χ^2
575	1.9	5.9×10^{-5}	–	1.2×10^{-2}	5.82	0.186	0.73	3×10^{-4}
650	2.3	1.1×10^{-4}	14.4	1.6×10^{-3}	15.6	0.064	0.75	5×10^{-4}
675	1.2	8.6×10^{-3}	4.10	1.8×10^{-2}	7.24	0.082	0.59	1×10^{-4}
695	1.1	–	–	–	1.90	0.108	0.72	8×10^{-5}

Fig. 5. Equivalent circuit used for impedance analysis of type 310S stainless steel. R_Ω: electrolyte resistance; C_{dl}: double layer capacitance; R_{ct}: charge transfer resistance; C_f: oxide film capacitance; R_f: oxide film resistance; CPE: constant phase element.
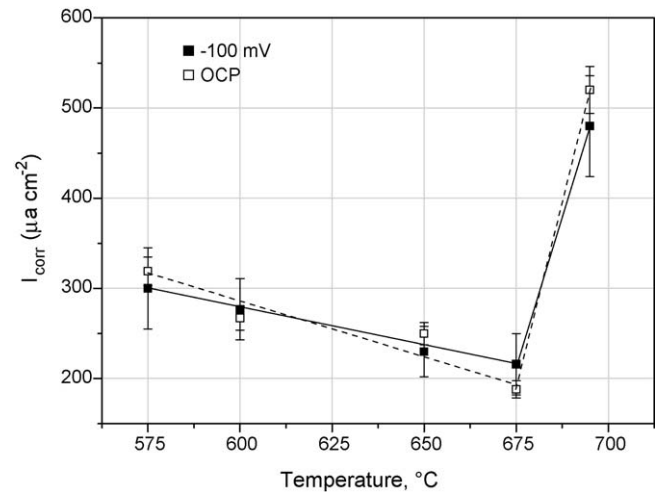

Fig. 6. Corrosion rate of type 310S stainless steel in the Li + K carbonate under load (−100 mV) and under stable OCP conditions. Atmosphere: standard cathode gas.

exponent n describes a diffusion-related element that becomes a capacitor for $n = 1$ or a Warburg resistance for $n = 0.5$. For intermediate values of n, CPE may represent an oxide growth process taking place prevalently through a finite diffusion length. At 650 and 675 °C a charge transfer resistance (R_{ct}) value could be determined indicating that for the passive steel the interfacial charge transfer process becomes sufficiently slow to be detected. However, the barrier properties of the passive film are not fully satisfactory as indicated by the diffusion response still observable at low frequencies. The low values of CPE element (inverse of Q) state for a rapid kinetics of the oxide growth. The CPE and oxide film (R_f) resistances were both observed to decrease from 650 °C onwards. A possible explanation for these findings could be an accelerated oxide growth due to increasing Li$^+$ inward diffusion stimulated by the higher temperatures with a consequent reduction of the electrical resistance of the lithiated oxide.

3.5. Corrosion rate determinations

The corrosion current was measured under load (at the cathode potential (−100 mV)) and under stable OCP conditions. For the first type of measurements, the current was monitored potentiostatically for two hours and a reference value was taken after 1 h. For the second type of measurements, the corrosion current was estimated by extrapolation at zero-current of the anodic Tafel branch of the polarization curve. The results are presented in Fig. 6 as a function of temperature. At both the potentials the corrosion rate showed a similar trend. After reaching a minimum at 675 °C, the corrosion increased rapidly as the temperature approaches 695 °C.

3.6. XRD spectra

From the previous results it could be deduced a change in the corrosion mechanism from 575 to 600 °C at which temperature the steel became fully passive at OCP. In order to identify

the corrosion products associated with the passivation process, selected electrode surfaces were analyzed by XRD after OCP experiments. A depth profile composition of the oxide scale was obtained by determining XRD spectra on as-received samples and also after a light polishing to remove about 5 μm of the surface (see Fig. 7). The corrosion product at 650 °C is composed by a surface iron oxide layer consisting of external $LiFeO_2$ and underneath $LiFe_5O_8$ phase and an inner layer of $LiCrO_2$. At 575 °C, the $LiFe_5O_8$ phase is the predominant constituent with no evidence of the $LiCrO_2$, thus suggesting that $LiFe_5O_8$ at 575 °C is much thicker than at 650 °C. It is well known that only $LiFeO_2$ may form a dense and compact layer to ensure a rather good passivity, whereas $LiFe_5O_8$ is too porous to provide adequate corrosion resistance in carbonate melts. Thus, the passage from active to passive state observed in the anodic polarization scan logically could be the consequence of the following phase transition from $LiFe_5O_8$ to $LiFeO_2$:

$$LiFe_5O_8 + 3Li^+ = 4LiFeO_2 + Fe^{3+} \qquad (1)$$

As this reaction must take place at the inner $LiFe_5O_8/LiFeO_2$ interface, this obviously requires some inward diffusion of Li$^+$ ions through the external part of the oxide to make this reaction possible. It is likely that Li$^+$ diffusion occurs simultaneously with the Ni^{2+} oxidation process:

$$Ni^{2+} = Ni^{3+} + e^- \qquad (2)$$

Assuming a Ni-containing oxide scale, this redox process probably might induce the formation of lattice vacancies through which Li ions could accomodate in the oxide structure and make them available for the lithiation of $LiFe_5O_8$ phase. The proposed model is reasonable considering that the Ni^{2+}/Ni^{3+} potential is reported at about −450 mV [7], which is well in accordance with the position of the active–passive peak observed in the polarization scan curves and also with the findings of potential decay measurements.
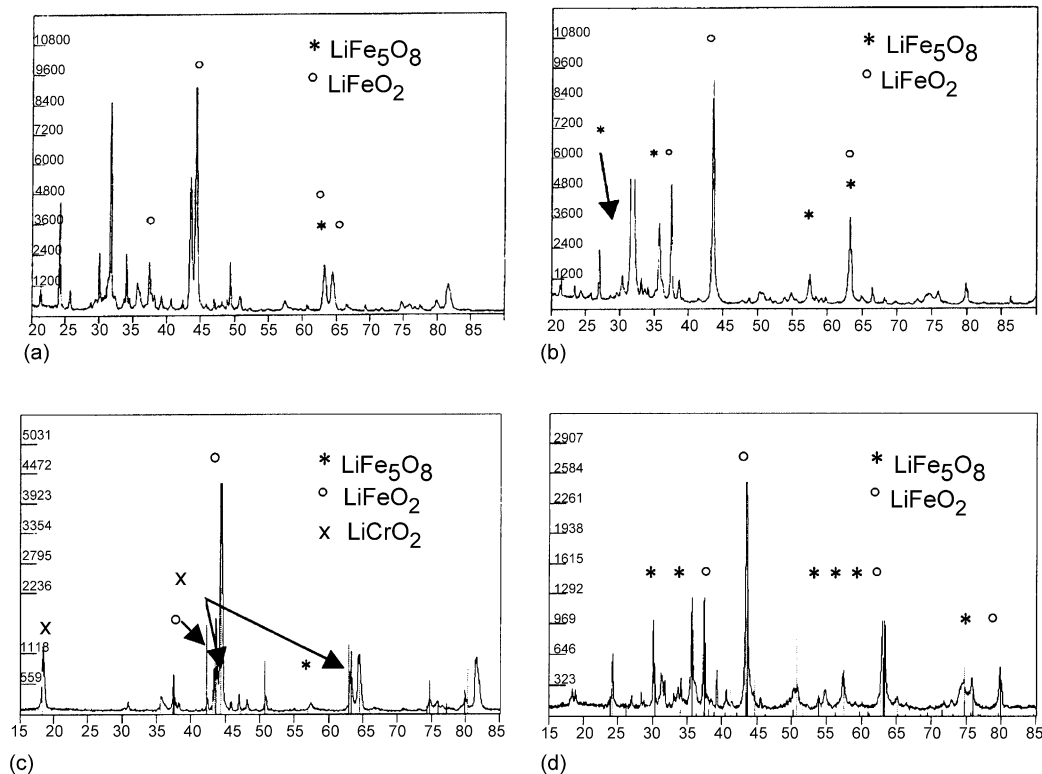
Fig. 7. XRD spectra of type 310S stainless steel samples corroded in the Li + K carbonate until attainment of stable OCP conditions: (a) 650 °C, not polished; (b) 575 °C, not polished; (c) 650 °C, after polishing; (d) 575 °C, after polishing. Atmosphere: standard cathode gas.

4. Summary

The main results of this work may be summarized as follows:

1. The corrosion behavior of type 310S stainless steel in the eutectic Li + K carbonate melt is significantly affected by temperature. Below 600 °C and above 675 °C a stable passive behavior could not be attained due to a prevalent formation of porous $LiFe_5O_8$ (at least, below 600 °C) in place of the more protective and stable $LiFeO_2$.
2. The temperature dependency of corrosion rate showed a similar trend under OCP and load conditions with a minimum rate at 675 °C.
3. By combining electrochemical measurements and XRD analysis of corrosion products it has been proposed a plausible mechanism to explain the active–passive transition observed in the anodic polarization scans based on the lithiation of the $LiFe_5O_8$ phase to form $LiFeO_2$. The Li^+ inward diffusion

process could be facilitated by the concomitant oxidation of Ni^{2+} ions present in the oxide structure.

References

[1] A. Schoeler, T.D. Kaun, I. Bloom, M. Lanagan, M. Krumpelt, J. Electrochem. Soc. 147 (2000) 916–921.
[2] K. Ota, K. Toda, S. Mitsushima, N. Kamiya, Bull. Chem. Soc. Jpn. 75 (2002) 877–881.
[3] P. Biedenkopf, M.M. Bischoff, T. Wochner, Mater. Corros. 51 (2000) 287–302.
[4] T.H. Lim, E.R. Hwang, H.Y. Ha, S.W. Nam, I. Oh, S. Hong, J. Power Sources 89 (2000) 1–6.
[5] S. Frangini, in: J.R. Selman, I. Uchida, et al. (Eds.), Carbonate Fuel Cell Technology IV, PV 97-4, The Electrochemical Society Proceeding Series, Pennington, NJ, 1997, pp. 306–314.
[6] S. Frangini, Mater. Corros. 57 (2006) 330–337.
[7] M.S. Yazici, J.R. Selman, Solid State Ionics 124 (1999) 149–160.
[8] S.A. Salih, A.N. El-Masri, A.M. Baraka, J. Mater. Sci. 36 (2001) 2547–2555.